Low Impedance Fault Identification and Classification Based on Boltzmann Machine Learning for HVDC Transmission Systems

Raheel Muzzammel and Ali Raza

***Abstract*—Identification and classification of DC faults are considered as fundamentals of DC grid protection. A sudden rise of DC fault current must be identified and classified to immediately operate the corresponding interrupting mechanism. In this paper, the Boltzmann machine learning (BML) approach is proposed for identification and classification of DC faults using travelling waves generated at fault point in voltage source converter based high-voltage direct current (VSC-HVDC) transmission system. An unsupervised way of feature extraction is performed on the frequency spectrum of the travelling waves. Binomial class logistic regression (BCLR) classifies the HVDC transmission system into faulty and healthy states. The proposed technique reduces the time for fault identification and classification because of reduced tagged data with few characteristics. Therefore, the faults near or at converter stations are readily identified and classified. The performance of the proposed technique is assessed via simulations developed in MATLAB/Simulink and tested for pre-fault and post-fault data both at VSC1 and VSC2, respectively. Moreover, the proposed technique is supported by analyzing the root mean square error to show practicality and realization with reduced computations.**

***Index Terms*—Binary class logistic regression (BCLR), Boltzmann machine learning (BML), DC grid protection, fault identification and classification, voltage source converter based high-voltage direct current (VSC-HVDC) transmission system.**

I. Introduction

RECENTLY, renewable energy generation develops rapidly. Therefore, ample attentions are captured by voltage source converter based high-voltage direct current (VSC-HVDC) systems for power transmission. Reactive power support [1], black start capability [2], small filter size [3], and the ability to change the power direction without altering the polarity of the DC link voltage [4] make VSC-HVDC a viable candidate for multi-terminal HVDC rather than the technology of line commutated converter (LCC) [5], [6]. However, DC grid protection is a significant hindrance to the development of practical multi-terminal VSC-HVDC systems.

Typically, the DC grid protection is divided into two categories: fault diagnosis and fault interruption (FI). Fault diagnosis includes fault identification and classification (FIC) and fault location (FL). FIC is the leading research problem in the area of the VSC-HVDC system because of the abrupt rising nature of DC fault current, resulting in damaging the converter stations (CSs) [3], [7], [8]. Moreover, the FI technique can only be designed after FIC. We mainly focus on the new FIC based on the Boltzmann machine learning (BML) approach.

Normally, faults are located via impedance-based methods, compromising the accuracy as the fault distance varies on the transmission line (TL) with FL [9]. Therefore, FIC based on voltage and current samples is proposed but is affected by electrical noise and fault loop impedance [10], [11]. Since the aforementioned methods provide little information about FIC, travelling wave (TW) based FIC techniques are developed in [3], [8], [12]. Naturally, the maximum information is retrieved from the first TW wavefront [3]. However, the difficulty in the detection of the first TW wavefront leads to imprecisions [3], [7], [8]. The single-ended protection system is also designed to enhance the speed of FIC [13], but its application is limited to HVDC transmission systems comprising large capacitors in parallel. The DC fault protection based on transient voltage [14], frequency and time characteristics of fault current [15]-[17], electromagnetic time reversal (EMTR) [18], [19], Pearson similarity [20]-[22], *K* means classification [23], linear discriminant analysis [24], [25] are also proposed in literature. Further, with an introduction of the concept of time lag for the FL, the two-terminal measurement-based method is devised for FIC near CSs [22], [26], [27].

Knowledge-based methods like fuzzy logic [28], neural networks [29], Bayesian networks [6], and support vector machines [30] offer convincing benefits [3], [7]. Moreover, the accuracy of FIC is compromised for incomplete information and the analysis of complex power system [3].

The objectives of this paper are as follows: ① accurate FIC, even close to the VSC station; ② decrease in DC FIC time; ③ reduced tagged data; ④ reduced training time and dimensions of the feature space. Moreover, almost all of the techniques in literature fail to identify and classify the faults near or at CSs [1]-[4]. This is the main motive to consider

Manuscript received: July 7, 2020; revised: October 13, 2020; accepted: December 7, 2020. Date of CrossCheck: December 7, 2020. Date of online publication: March 9, 2021.

R. Muzzammel (corresponding author) and A. Raza are with the Department of Electrical Engineering, University of Lahore, Lahore 54000, Pakistan (e-mail: raheelmuzzammel@gmail.com; ali.raza@ee.uol.edu.pk).

DOI: 10.35833/MPCE.2020.000386

DC faults near or at CSs in this paper. Furthermore, voltage measurements are used to analyze the normal and faulty states of the HVDC transmission system.

In this paper, the BML-based approach is proposed for FIC in the HVDC transmission system. BML performs unsupervised feature extraction by selecting a small time frame from the spectrum [31]-[38]. BML-based FIC is not presented in the literature. TWs generated at fault points are employed for the preparation of training and testing data. Feature extraction for the pole-to-pole fault identification is carried out on the frequency spectrum of TWs using BML. Binomial class logistic regression (BCLR) is employed to classify the HVDC transmission system into faulty and healthy states. BCLR works on the dimensionally reduced data for classification [39], [40]. Moreover, the realization of the proposed technique is supported by the root mean square analysis. Although the FIC methodology is tested for a two-terminal HVDC transmission system, it can be extended to multi-terminal systems.

The rest of the paper is organized as follows. Section II and Section III briefly describe the structure and mathematical formulation of BML and BCLR. The detailed design of the algorithm of FIC is added in Section IV. Section V provides a brief description of the DC test grid under study. The simulation results of the test system for the validation of the proposed technique are presented in Section VI. Finally, conclusions are drawn in Section VII.

II. BML

The BML is a stochastic learning method with reduced featured data [31]-[38]. Testing and training data are prepared from random values, which serve as the initiation for the influencing factors of BML. Many training examples and excessive iterative approaches are required for random initialization of the influencing factors of BML to obtain the global minima of its objective function. Only local minima are achieved with the help of a few training data. This results in the inconsistency of learned features and influencing factors. As a result, the performance of identification and classification is compromised. Therefore, to cope with this situation, these random influencing factors are initiated with the values that have the features closer to the training data.

Training is a two-step process in BML. In the first step, BML-X is trained on the untagged data, which learns features from the data. These untagged features serve as the initial influencing factors for the second step, i.e., BML-Y. The training of BML-Y is done with initial influencing factors and tagged training data. Thus, the global minima of the objective function of BML-Y are obtained within a short time and with few training data. This learning approach for an untagged data is known as self-taught learning [41].

The untagged data, i.e., unknown fault class, is termed as an unknown classification of TW data. The tagged data, i.e., known fault class, is termed as the known classification of TW data, as shown in Fig. 1. The untagged and tagged data may originate from the same source. Practically, it is not feasible to gather data of a particular type of faults from several HVDC transmission systems. However, it is easier to collect data of faults from an HVDC transmission system for which fault tags are unknown. A regression classifier is further employed for the classification of training and testing data [42].

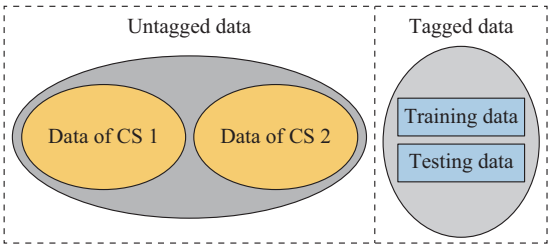

Fig. 1. Organization of tagged and untagged TW data for BML.

BML possesses hidden and visible layers. The energy of the hidden and the visible layers $E(p,q)$ are calculated as:

$$E(p,q) = -ap - bq - q\boldsymbol{W}p \tag{1}$$

where p and q denote the visible and the hidden layers, respectively; a and b are the biases of the elements of visible and hidden layers, respectively; and $\boldsymbol{W}$ is an influencing factor of the link between the elements of visible and hidden layers. The joint probability of the elements of hidden and visible layers $P(p,q)$ is:

$$P(p,q) = \frac{1}{Z}\mathrm{e}^{E(p,q)} \tag{2}$$

where Z is a partition function. It is presented as a sum of the energies of all possible configurations:

$$Z = \sum_{p,q}\mathrm{e}^{E(p,q)} \tag{3}$$

The activation of a particular q for a visible layer status v is defined by conditional probability $P(q=1|p)$ as:

$$P(q=1|p) = \sigma\left(\boldsymbol{W}^{\mathrm{T}}q + b\right) \tag{4}$$

where σ is a logistic function. Similarly, the activation of p for q is:

$$P(p=1|q) = \sigma\left(\boldsymbol{W}^{\mathrm{T}}p + a\right) \tag{5}$$

The training parameters of BML, W, a, and b are carried out by contrastive divergence (CD) [43]. In this paper, the structures of BML-X and BML-Y are precisely the same. Linear transformation of input training data $\boldsymbol{x}_l$ and testing data $\boldsymbol{x}_t$ into the reduced dimensional vector is carried out by $\boldsymbol{W}$ as:

$$\boldsymbol{X}_l = \boldsymbol{W}_2^{\mathrm{T}}\boldsymbol{x}_l \tag{6}$$

$$\boldsymbol{X}_t = \boldsymbol{W}_2^{\mathrm{T}}\boldsymbol{x}_t \tag{7}$$

where $\boldsymbol{x}_l$ and $\boldsymbol{x}_t$ are the transformed vectors. $\boldsymbol{x}_l$ is applied to train the BCLR discussed in the subsequent section. Reduced training vectors optimize the objective function of classification rapidly. Hence, the performance of BML is improved.

III. BCLR

BCLR has a dependent variable that has two possible val-

ues tagged as 0 or 1. In the logistic model, the logarithm of the log odds for the value tagged "1" is a linear combination of one or more independent variables (predictors). Independent variables can be binary variables, i.e., two classes, coded by an indicator variable, or a continuous variable with any real value. The probability of the value tagged as "1" has the probability of either 0 or 1. A sigmoid function maps the predicted values to the probabilities. Any real value can be mapped into another value that exists between 0 and 1. A threshold point is chosen, which serves as a decision boundary for the classification. BCLR is extended to more than two levels of the dependent variables. Less training data for feature extraction and less computation time are the notable advantages as compared with fuzzy logic [28], neural networks [29], [30], Bayesian networks [6], and support vector machines based classification [31], [39], [40].

The relationship between output values of BML and BCLR is given in (8) for joint probability.

$$P\left(y=1|\boldsymbol{X}_l\right)=\frac{1}{1+\mathrm{e}^{SX_l+T}} \tag{8}$$

where S is the influencing factor and T is the bias, which are trained by the maximum likelihood problem. The objective function of the maximum likelihood problem $F(S,T)$ is:

$$F(S,T)=\min\left(-\sum_{i=1}^{n}t_i\lg\left(p_i\right)+\left(1-t_i\right)\lg\left(1-p_i\right)\right) \tag{9}$$

where p_i is the probability of $\boldsymbol{x}_l$ and is given by (10); and the threshold t_i is given by (11).

$$p_i=\frac{1}{1+\mathrm{e}^{SX_l\left(\boldsymbol{x}_l\right)+T}} \tag{10}$$

$$t_i=\begin{cases}\dfrac{N_+ +1}{N_+ +2} & i=1,2,\ldots,n\\ \dfrac{1}{N_- +2} & i=1,2,\ldots,n\end{cases} \tag{11}$$

where N_+ and N_- are the positive and negative class numbers, respectively. The generalized structure of the proposed technique based on BML and BCLR is presented in Fig. 2.

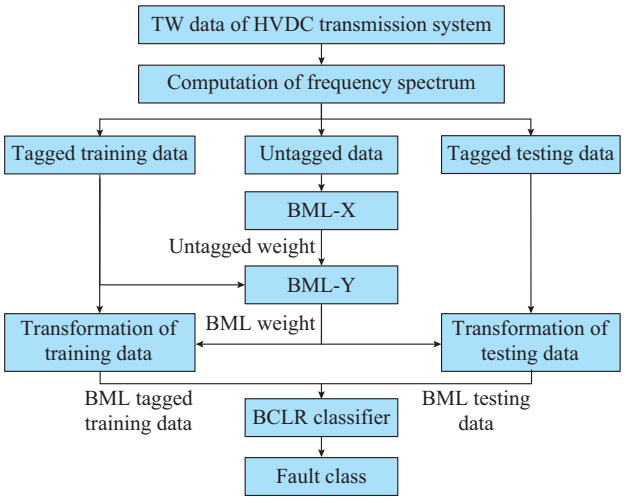

Fig. 2. Structure of proposed technique based on BML and BCLR.

The possible structure of BML-based protection scheme is presented in Fig. 3. Influencing factors trained by BML are fed as an input of primary relay and backup relay. The tripping mechanism of relay works based on the threshold analysis of root mean square error (RMSE). The backup relay follows relay coordination properly by considering the operation of the primary relay and circuit breaker (CB).

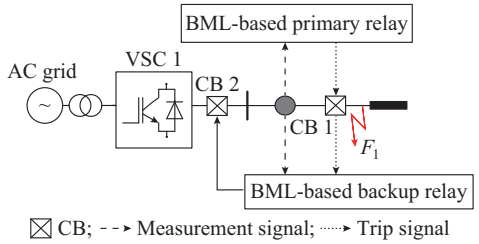

Fig. 3. Possible structure of BML-based protection scheme.

IV. BML and BCLR Based FIC

Tagged and untagged data are generated from the frequency spectrum under pre-fault and post-fault conditions as shown in Supplement Material A, Fig. A1. The training of the BML is carried out in two stages, as explained in Section II. In the first stage, untagged data are fed as an input to the BML algorithm, resulting in the extraction of untagged influencing factors. Untagged influencing factors are converted to tagged influencing factors in the second stage. These tagged influencing factors are then used to transform the training data and testing data as tagged training data and tagged testing data, respectively. The transformed data are then used by BCLR to classify the faults as shown in Supplement Material A, Fig. A2. The algorithm for identifying the state of a test system based on types of data transformation is presented in Fig. 4. DC faults are classified in terms of faults at CS 1 and CS 2, respectively.

The proposed technique is validated with an analysis of RMSE. True response and predicted response are evaluated for RMSE, as shown in Supplement Material A, Fig. A3. Furthermore, RMSE is fed to BCLR to classify the faults, as presented in Fig. 5.

V. VSC-HVDC Test System Under Study

A single-line diagram of the proposed two-terminal VSC-HVDC test system is shown in Fig. 6. Positive and negative DC voltages are considered in the bi-polar system. At an onshore VSC station, fixed DC voltage and reactive power controls are employed to control the DC voltage [18]. At an offshore VSC station, the P-V_{AC} control mode is set. With these arrangements, constant active power flow is assured across the power grid, and the AC voltage level is regulated at the point of common coupling (PCC) [43]. The dq control approach [43] is employed at the primary level. An average two-level VSC value model is used for HVDC modelling, while the wind farm is demonstrated as a fixed power source. Parameters of the VSC-HVDC test system and DC link are presented in Table I and Table II, respectively.

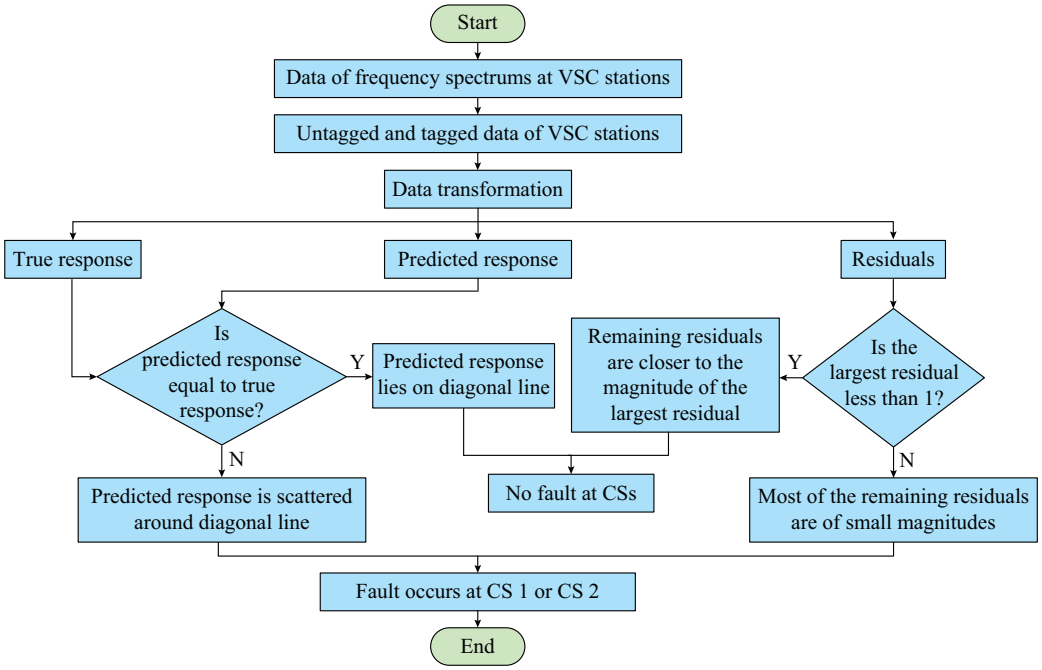

Fig. 4. Algorithm for identification of normal and faulty states of HVDC transmission system.

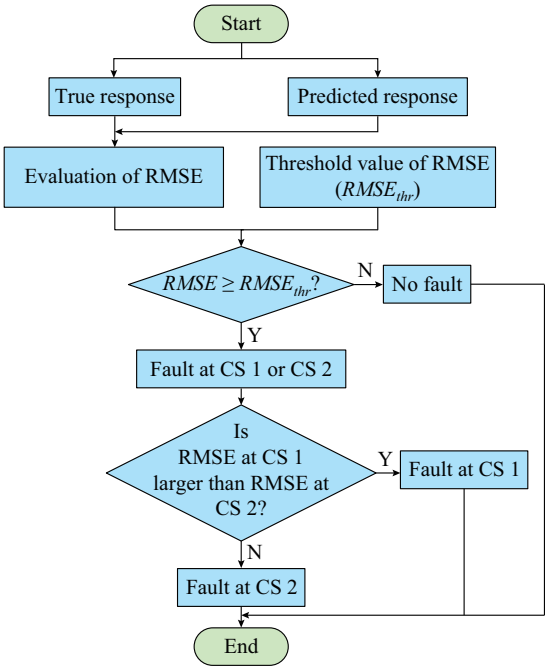

Fig. 5. Algorithm for classification of faults in HVDC transmission system.

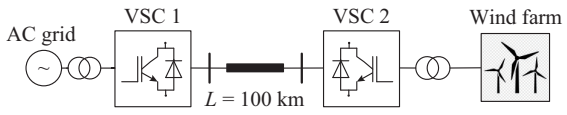

Fig. 6. VSC-HVDC test system under study.

VI. Simulation

The performance of the proposed BML and BCLR for the FIC is tested on the VSC-HVDC test system of Fig. 6. The data for training and testing are prepared from the TWs in healthy and faulty states of the DC grid.

TABLE I
Parameters of VSC-HVDC Test System

Parameter	VSC 1	VSC 2
Power (MVA)	2000	2000
AC voltage (kV)	230	230
DC voltage (kV)	±100	±100
Nominal frequency (Hz)	50	50
Switching frequency (kHz)	1350	1350
Reactive power of AC filter (Mvar)	40	40
Phase reactor (p.u.)	0.150	0.150
DC capacitance (μF)	70	70
Smoothing reactor (Ω)	2.510	2.510

TABLE II
Parameters of DC Link in VSC-HVDC Test System

Parameter	Value
DC line length (km)	100
DC line resistance (Ω/km)	0.0139
DC line inductance (mH/km)	0.16
DC line capacitance (μF/km)	0.23
Number of pi-sections	2

The classification of the conditions is conducted by majority voting-based criteria among faulty and healthy states. Voltages are observed at VSCs/CSs to explain the behaviour of test system under pre-fault and post-fault conditions, as shown in Supplement Material A, Fig. A4.

A. DC Voltage Analysis

The voltage data pattern of VSC-HVDC test system under no-fault condition are shown in Fig. 7. Sub-transient and transient voltages are recorded before 2.5 ms because DC

voltages achieve steady-state value (1 p.u.) within approximately 2.5 ms at both CSs, which depicts the normal conditions of the HVDC transmission system. Transients are decayed down because of DC capacitors and the deployment of DC filters that are used to eradicate the harmonic contents.

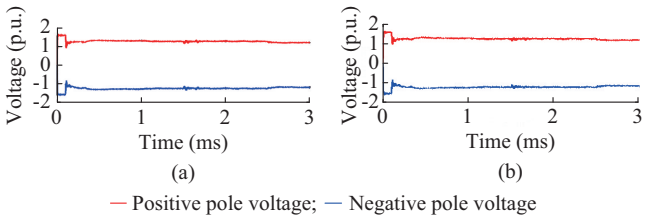

Fig. 7. Voltage data patterns of VSC-HVDC test system under no-fault condition. (a) VSC 1. (b) VSC 2.

When a pole-to-pole fault of DC occurs in the VSC-HVDC test system, the variations in voltage profiles at VSC 1 and VSC 2 are recorded and presented in Fig. 8. Voltages are reduced to zero in less than 0.5 ms. It means that the DC fault current achieves the maximum steady-state value in less than 0.5 ms, which is highly vulnerable. Therefore, DC fault current needs to be interrupted before attaining the maximum value. It is only possible if FIC is carried out within permissible time. Healthy and faulty states of an HVDC transmission system can be easily identified with the help of voltage measurements. However, it is difficult to classify the fault with only voltage measurements due to similar decaying voltage patterns at both VSC 1 and VSC 2. Therefore, more in-depth investigations are required to analyze the features.

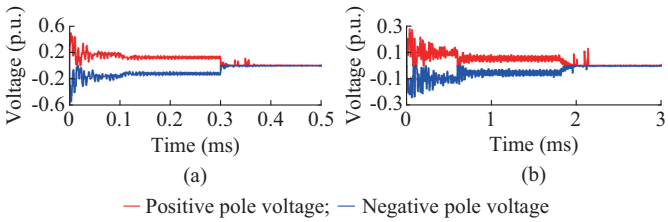

Fig. 8. Voltage data patterns of VSC-HVDC test system under faulty condition. (a) VSC 1. (b) VSC 2.

B. Frequency Analysis

Frequency analysis is used to extract the information available in the variations of voltages at CSs, as shown in Supplement Material A, Fig. A5. Frequency spectrum patterns of VSC-HVDC test system under no-fault condition for CSs are shown in Fig. 9.

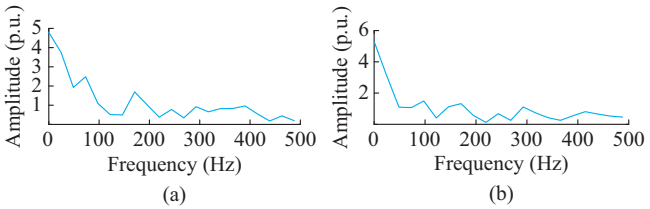

Fig. 9. Frequency spectrum patterns of VSC-HVDC test system under no-fault condition. (a) VSC 1. (b) VSC 2.

However, it is observed that the decaying pattern is different in different ranges of frequencies observed at CS 1 and CS 2. In the range of frequencies of 50-100 Hz, the first rise of 2 p.u. is experienced for CS 1, as shown in Fig. 9(a), while the first rise for CS 2 is of 1 p.u. as shown in Fig. 9(b). In the range of frequencies of 300-400 Hz, a small change in the amplitude is observed for CS 1, as shown in Fig. 9(a), while a significant decay in the amplitude is observed for CS 2. This information helps identify untagged data observed in the VSC-HVDC test system, which is used in the first step training of BML. Decaying patterns of the frequency spectrum are also observed at CSs under the faulty condition, as shown in Fig. 10. In the range of frequencies from 200 Hz to 250 Hz, a clear difference in the characteristic curves of frequency for CSs can be observed in Fig. 10. A decay with a small change in amplitude is observed for a DC fault close to CS 2, while a significant change in amplitude is recorded for a DC fault close to CS 1. The difference in the characteristics of the frequencies is employed for FIC.

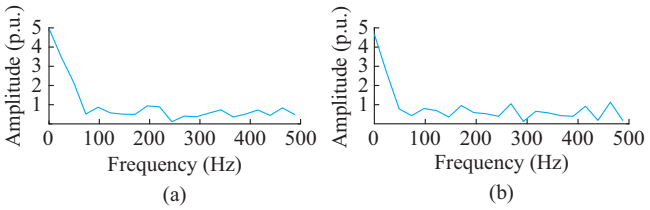

Fig. 10. Frequency spectrum patterns of VSC-HVDC test system under faulty condition. (a) VSC 1. (b) VSC 2.

C. Different Cases of VSC-HVDC Test System

Various cases are performed on an VSC-HVDC test system of Fig. 6, as shown in Table III. In the following graphical results, blue dots represent true response (TR), while red dots represent predicted response (PR).

TABLE III
DIFFERENT CASES OF VSC-HVDC TEST SYSTEM BASED ON TRAINING AND TESTING DATA

Case	CS	Testing data
1	CS 1	Pre-fault data of CS 1
2		Post-fault data of CS 1
3		Pre-fault data of CS 2
4		Post-fault data of CS 2
5	CS 2	Pre-fault data of CS 2
6		Post-fault data of CS 2
7		Pre-fault data of CS 1
8		Post-fault data of CS 1

1) Case 1

In case 1, untagged data are fed into BML-X, as shown in Fig. 11(a). Untagged influencing factors obtained are provided into BML-Y along with the tagged training data of CSI. PR obtained from the BML is precisely matching the tagged data of CS 1 under the no-fault condition, as shown in Fig. 11(b). The perfect regression model pattern of PR against TR is obtained, as shown in Fig. 12(a). As a result, all

points lie on the line. Residuals of PR against the frequency are symmetrical about an axis, as shown in Fig. 12(b). Thus, it is identified that CS 1 of the VSC-HVDC test system is under no-fault condition.

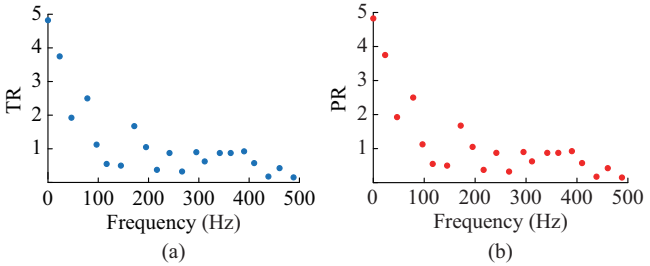

Fig. 11. Untagged and tagged data pattern in case 1. (a) Untagged data pattern of CS. (b) Tagged data pattern of CS 1 under no-fault condition.

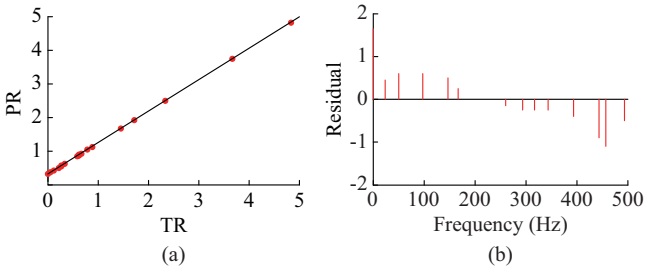

Fig. 12. TR and PR in case 1. (a) TR and PR patterns under no-fault condition. (b) Residual PR pattern against frequency to depict performance.

2) Case 2

In case 2, the proposed technique is trained with untagged data and is tested for post-fault tagged data of CS 1. A significant difference between PR and TR patterns of post-fault exists, as shown in Fig. 13(a). Larger values of RMSE (0.56425) mean that PR and TR are not following a similar pattern. Imperfections are indicated as shown in Fig. 13(b), which leads to the differences between TR and PR. Outliers occur as shown in Fig. 13(c), which means that few residuals are more extensive in the magnitude than the rest of the outliers. RMSE is sensitive to outliers. A clear non-linear pattern is observed in Fig. 13(c), which depicts the difference between PR and TR, resulting in FIC at CS 1.

3) Case 3

In case 3, untagged data of CS are used to train BML-X. Then, the tagged data of CS 1 are used to train BML-Y. The data of CS 2 are used to test an algorithm. A difference between TR and PR is observed, as shown in Fig. 14(a). Few points lie on the line as shown in Fig. 14(b). The non-linear pattern of residuals is observed in Fig. 14(c), which indicates that TR belongs to the data of CS 1 obtained after the training algorithm and PR belongs to the data of CS 2 obtained after the testing algorithm. As a result, the large value of RMSE (0.45087) indicates the difference between PR and TR, leading to the identification of normal states of CS 1 and CS 2. Moreover, the RMSE value is less than the threshold RMSE, i. e., 0.5, leading to the discrimination between normal and faulty states of the VSC-HVDC test system, as depicted in Fig. 5.

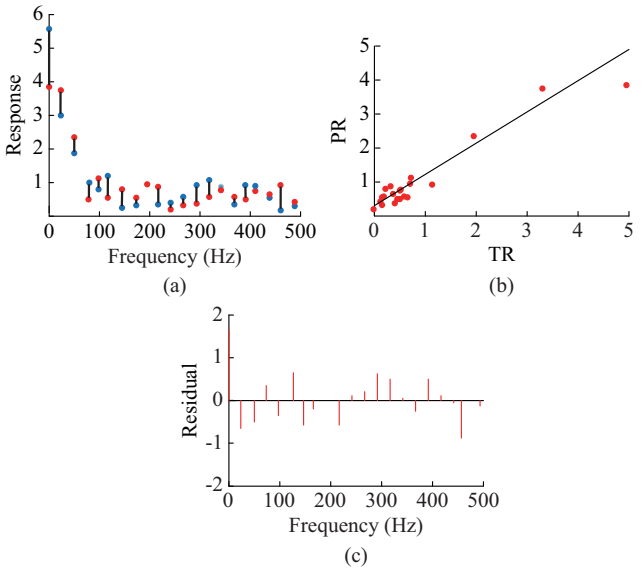

Fig. 13. Characteristics of PR in case 2. (a) PR of fault and TR of VSC 1 plotted against frequency. (b) PR against TR of VSC 1. (c) Residuals of PR in post-fault state of VSC 1 against frequency to depict performance of trained model.

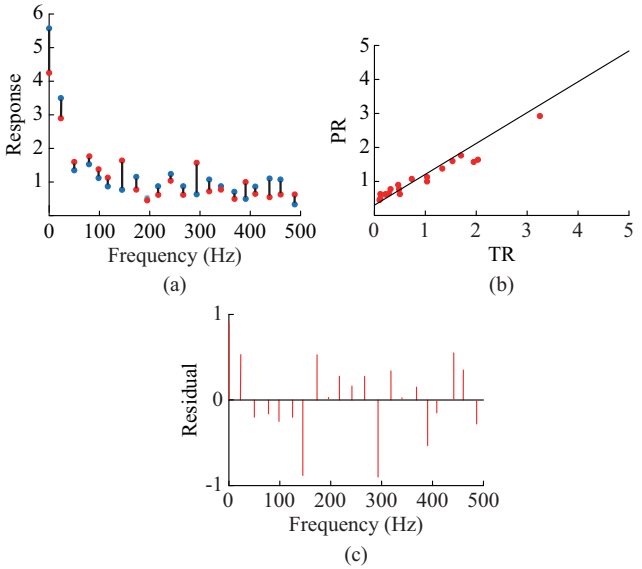

Fig. 14. Characteristics of PR in case 3. (a) PR of VSC 2 and TR of VSC 1 plotted against frequency. (b) PR of VSC 2 against TR of VSC 1. (c) Residuals of PR of VSC 2 against frequency to depict performance of trained model.

4) Case 4

In case 4, the proposed technique is trained with the data of CS 1 and tested with the tagged data under the post-fault condition of CS 2. The difference between TR and PR indicates the discrimination between training and testing data, as shown in Fig. 15(a). Scattered points below and above the line indicate that the trained algorithm is imperfect for testing data, as shown in Fig. 15(b). RMSE value is larger than the threshold value of RMSE, i. e., 0.5, but is less than the RMSE value observed at CS 1. These observations lead to the FIC based on the fault at CS 1 and CS 2. The larger val-

ues of RMSE indicate the presence of outliers in the residuals plot, as shown in Fig. 15(c).

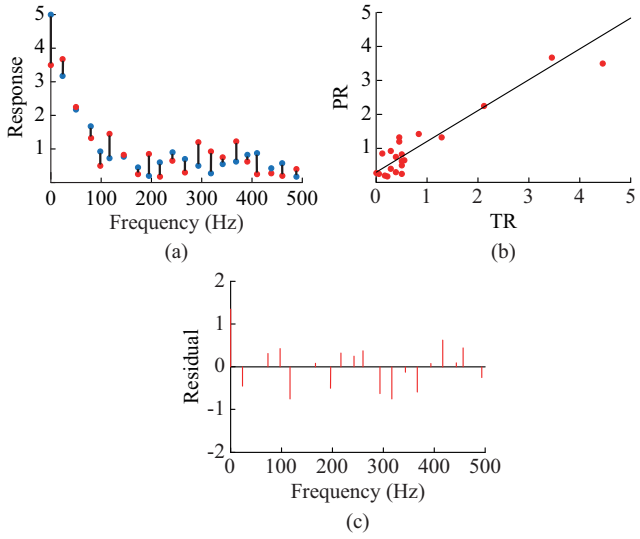

Fig. 15. Characteristics of PR in case 4. (a) PR of post-fault of VSC 2 and TR of VSC 1 plotted against frequency. (b) PR of post-fault condition of VSC 2 against TR of VSC 1. (c) Residuals of PR in post-fault state of VSC 2 against frequency.

5) Case 5

In case 5, tagged data of CS 2 are used for training and testing, as shown in Fig. 16(a). PR follows the pattern of TR, as shown in Fig. 16(b). Matching of PR with TR indicates that PR represents the data of CS 2, as shown in Fig. 17(a). Residuals are symmetrical about an axis, indicating the similarity between TR and PR, as shown in Fig. 17(b).The small values of RMSE are an indication of the presence of less sensitive outliers, which help identify the normal state of CS 2.

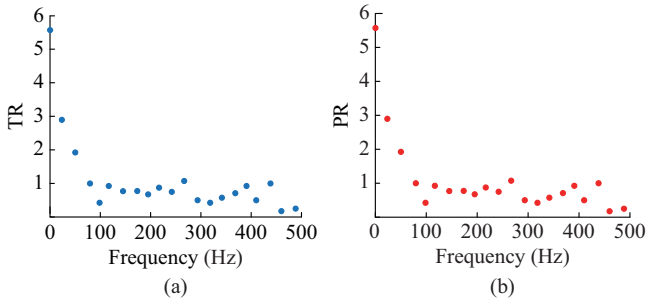

Fig. 16. Data patterns in case 5. (a) Untagged data pattern. (b) Predicted data pattern of VSC station.

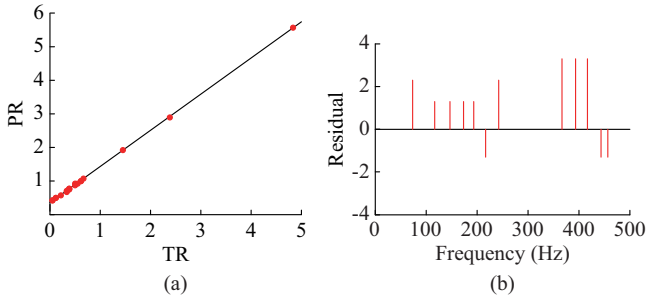

Fig. 17. Characteristics of PR in case 5. (a) TR of VSC 2 and PR. (b) Residuals of PR of VSC 2 against frequency to depict performance of trained algorithm.

6) Case 6

In case 6, the post-fault data of CS 2 are used to validate the performance of the proposed technique trained on untagged data. The difference between TR and PR is observed in Fig. 18(a). This is an indication that the training data and testing data are different. Because of scattered values below and above the line in Fig. 18(b), the TR of CS 2 is different from PR. Larger values of unsymmetrical residuals are another indication of the fault at CS 2, as shown in Fig. 18(c). RMSE value is greater than the threshold value of RMSE, which is an indication of the fault at CS 2 of the VSC-HVDC test system. In the event of a fault, the RMSE value at CS 2 is lower than the RMSE value at CS 1.

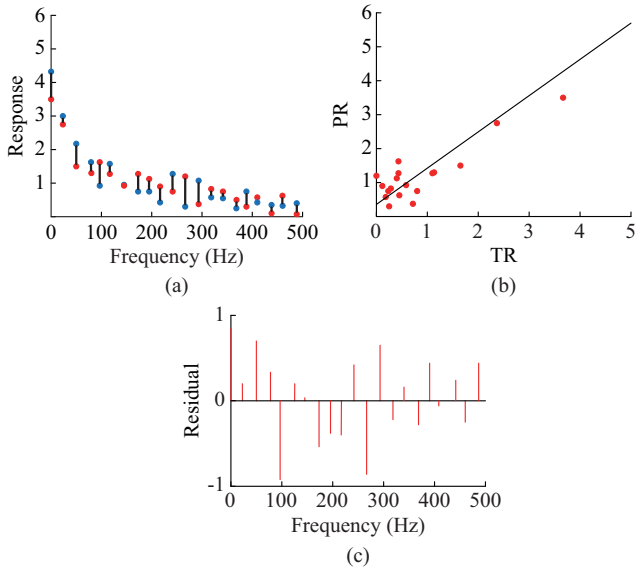

Fig. 18. Characteristics of PR in case 6. (a) PR of post-fault of VSC 2 against response of VSC 2. (b) PR of post-fault condition of VSC 2 plotted against TR of VSC 2. (c) Residuals of PR of post-fault state of VSC 2 against frequency.

7) Case 7

In case 7, tagged data of CS 1 under pre-fault condition are applied to test an algorithm trained on CS 2 data. Differences between the PR of CS 1 and data of TR of CS 2 are observed and shown in Fig. 19(a) and (b), respectively. Points are scattered below and above the line. Unsymmetrical residuals are recorded, as shown in Fig. 19(c). RMSE value (0.44706) is less than the threshold value of RMSE. Based on the dissimilarity between TR and PR and a smaller value of RMSE, no-fault is identified at CS 1 based on the training of BML with the data of CS 2.

8) Case 8

In case 8, the data of CS 2 are employed to train the proposed technique and are tested with the post-fault data of CS 1. The differences between TR and PR are substantial and recorded in Fig. 20(a) and (b), respectively, which lead to FIC. The magnitude of the largest residual is greater than 1. Smaller magnitudes of the remaining residuals indicate a fault in CS, as shown in Fig. 20(c). Based on the comparison of RMSE, it is found that the fault occurs at CS 1. The test system is summarized in Table IV, and the observations and results of BML and BCLR are summarized in Fig. 21.

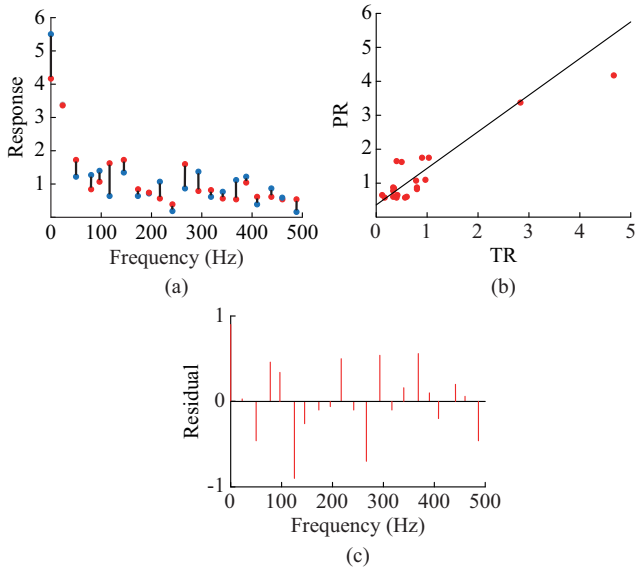

Fig. 19. Characteristics of PR in case 7. (a) PR of VSC 1 and TR of VSC 2 plotted against frequency. (b) PR of VSC 1 against TR of VSC 2. (c) Residuals of PR of VSC 1 against frequency.

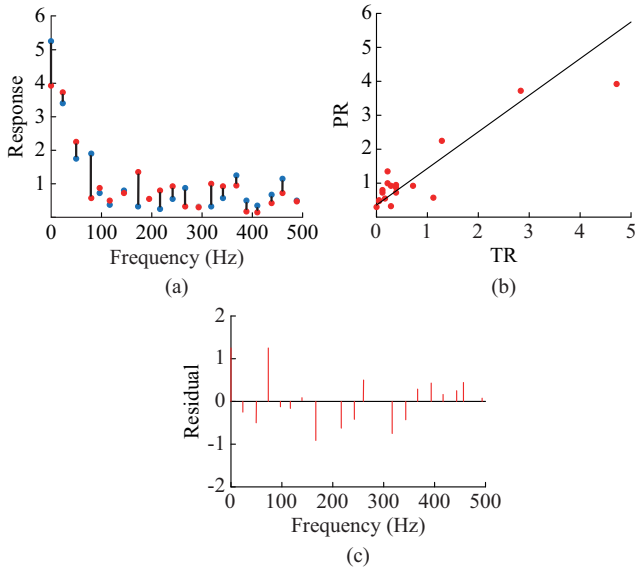

Fig. 20. Characteristics of PR in case 8. (a) PR of post-fault of VSC 1 and TR of VSC 2 plotted against frequency. (b) PR of post-fault condition of VSC 1 against TR of VSC 2. (c) Residuals of PR in post-fault state of VSC 1 against frequency.

TABLE IV
SUMMARY OF RESULTS FOR VARIOUS CASES OF TEST SYSTEM

Case	BML (untagged data)	BCLR (transformed data in fault class)	RMSE	MAE	Prediction time (s)	Training time (s)	FIC time (ms)
1	Amplitude of frequency spectrum values	No-fault	5.8274×10^{-16}	3.7668×10^{-16}	350	5.8895	2.85
2		CS 1 fault	0.56425	0.41352	460	4.7455	2.17
3		No fault	0.45087	0.36529	290	3.9169	3.40
4		CS 2 fault	0.50965	0.39805	360	3.4066	2.77
5		No-fault	1.5701×10^{-16}	1.0574×10^{-16}	360	3.5554	2.77
6		CS 2 fault	0.49906	0.42459	290	4.4860	3.40
7		No-fault	0.44706	0.35378	370	3.3629	2.70
8		CS 1 fault	0.55446	0.40725	290	6.6462	3.40

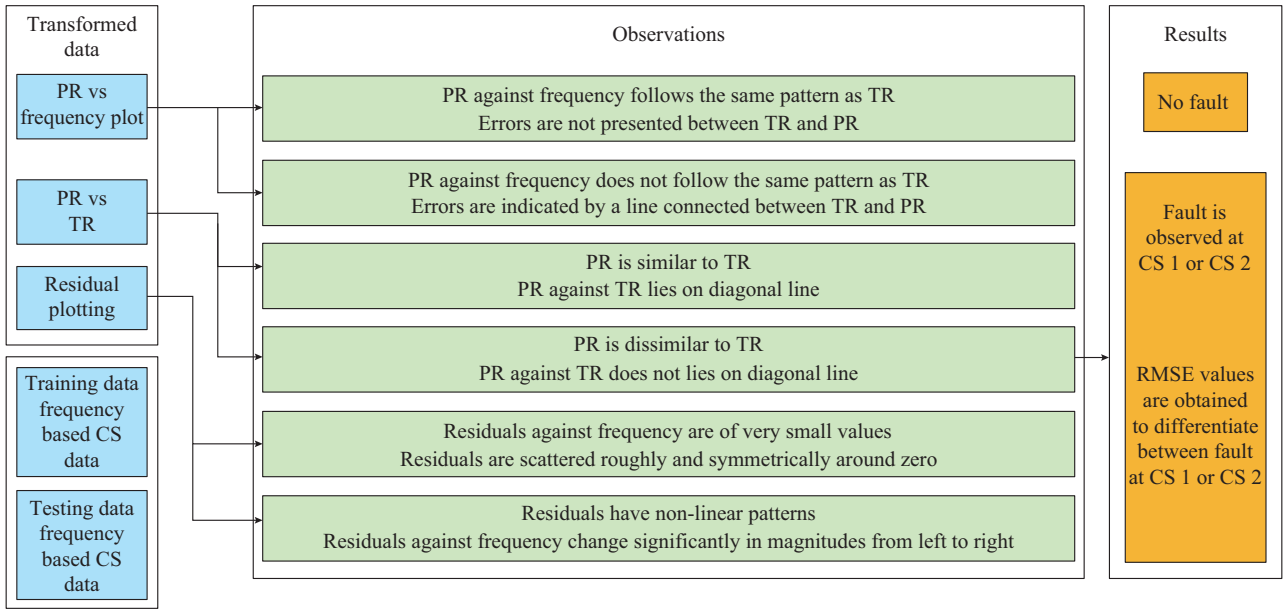

Fig. 21. Summary of observations and results obtained from eight different cases of test system.

D. Annotations of Proposed Technique for DC FIC

The benefits of the proposed technique for FIC are presented as follows.

1) The improvements in response time and fault classification are found as compared with the methods in [13], [22], [27].

2) The problem of fault detection with small arrival time characteristics at the sensing terminal is solved by BML with BCLR owing to advanced frequency-based features of TW for FIC.

3) Complexities and computations of FIC are reduced by the incorporation of RMSE in BML with BCLR.

4) Voltage measurements are highly recommended for FIC in faults of low-impedance DC grids.

E. Performance Comparisons

A detailed comparison of the proposed technique with different FICs in literature is presented in Table V.

TABLE V
COMPARISON OF DIFFERENT FIC TECHNIQUES

Parameter	Proposed method	TW-based single-terminal measurement-based method	TW-based two terminals measurement-based method	AI Techniques
Arrival time measurement	Not required	Required and influenced by line parameters	Required and influenced by line parameters. The difference between arrival times at both terminals must be acknowledged	Not required
Faults at CSs or near to VSC stations	Readily identified and classified	Not applicable. Additional approaches (wavelet transform, Fourier transform, S transform) are required	Not applicable and additional approaches (wavelet transform) are required	Not applicable and additional transformations are required
Complexity	Implementation is relatively easy	Complex digital processing techniques are required for accurate FIC	Complex synchronization is required to deal with the fault transients	Complicated because of extensive data handling
Computation time	Rapid FIC; and simple computation of RMSE is required	Computation time is dependent upon complex and time-consuming computations but quicker than the two-terminal methods	Synchronization and complex mathematical evaluations for accurate FIC increase the computation time	Extensive computation time because of the involvement of large data for training
Length of time window	FIC is independent of the time window length; and 2 ms time is enough	Accuracy is dependent on the length of the time window; and a time window of 10 ms gives reasonable results	Change in wave speed exerts a significant influence on the length of the time window, which influences the accuracy of results	Relatively large for training
Accuracy	More accurate; and even CS faults are distinguished with high efficiency	Sampling frequency and noisy measurements, especially at CSs, cannot be distinguished effectively	Accuracy is greatly influenced by the change in wave speed and non-synchronization	Incomplete information and large power systems make artificial intelligence techniques less accurate

VII. CONCLUSION

The BML technique is proposed along with the BCLR for low-impedance FIC in the VSC-HVDC test system. The proposed technique operates well for TW data measured at terminals of DC link with increased accuracy even for a small tagged training data. Furthermore, external engineering is not required for feature extraction. The two-terminal VSC-HVDC test system is tested for eight different cases of tagged and untagged data for FIC. DC fault can be classified with accuracy, even for faults close to or at VSC station, which is revealed as a drawback of the methods in literature. Moreover, the realization and computation efficiency of the proposed technique are proven with the analysis of RMSE. The benefits to multi-terminal HVDC transmission systems are extended for both forward and backward fault classifications.

REFERENCES

[1] M. Raza, "Active and reactive power control of hybrid offshore AC and DC grids," *Automatika*, vol. 60, no. 4, pp. 432-442, Feb. 2019.

[2] D. Jovcic, "VSC HVDC application for AC grid support and operation with passive AC systems," in *High Voltage Direct Current Transmission: Converters, Systems and DC Grids*. Hoboken: Wiley, 2019, pp. 359-365.

[3] R. Muzzammel, A. Raza, M. R. Hussain *et al*., "MT-HVDC systems fault classification and location methods based on traveling and non-traveling waves – a comprehensive review," *Applied Sciences*, vol. 9, no. 22, p. 4760, Nov. 2019.

[4] P. Rodriguez and K. Rouzbehi, "Multi-terminal DC grids: challenges and prospects," *Journal of Modern Power Systems and Clean Energy*, vol. 5, no. 4, pp. 515-523, Jul. 2017.

[5] Q. Huai, "Backup-protection scheme for multi-terminal HVDC system based on wavelet-packet energy entropy," *IEEE Access*, vol. 7, pp. 49790-49803, Apr. 2019.

[6] A. Raza, A. Akhtar, M. Jamil *et al*., "A protection scheme for multi-terminal VSC-HVDC transmission systems," *IEEE Access*, vol. 6, pp. 3159-3166, Dec. 2018.

[7] R. Muzzammel, "Machine learning based fault diagnosis in HVDC transmission lines," in *Communications in Computer and Information Science*, vol. 932. Singapore: Springer, 2019, pp. 496-510.

[8] R. Muzzammel, "Traveling waves-based method for fault estimation in HVDC transmission system," *Energies*, vol. 12, no. 19, p. 3614, Sept. 2019.

[9] S. Das, S. Santoso, A. Gaikwad *et al*., "Impedance-based fault location in transmission networks: theory and application," *IEEE Access*, vol. 2, pp. 537-557, May 2014.

[10] S. Agarwal, A. Swetapadma, C. Panigrahi *et al*., "Fault analysis method of integrated high voltage direct current transmission lines for onshore wind farm," *Journal of Modern Power Systems and Clean Energy*, vol. 7, pp. 621-632, May 2019.

[11] M. Daisy, R. Dashti, and H. R. Shaker, "A new fault-location method for HVDC transmission-line based on DC components of voltage and current under line parameter uncertainty," *Electrical Engineering*, vol. 99, no. 2, pp. 573-582, Jul. 2017.

[12] D. Wang and M. Hou, "Travelling wave fault location principle for hybrid multi-terminal LCC-VSC-HVDC transmission line based on R-ECT," *Electrical Power and Energy Systems*, vol. 117, pp. 1-9, May 2020.
[13] G. Song, X. Chu, S. Gao *et al*., "A new whole-line quick-action protection principle for HVDC transmission lines using one-end current," *IEEE Transactions on Power Delivery*, vol. 30, no. 2, pp. 599-607, Apr. 2015.
[14] J. Liu, N. Tai, and C. Fan, "Transient-voltage-based protection scheme for DC line faults in the multiterminal VSC-HVDC system," *IEEE Transactions on Power Delivery*, vol. 32, no. 3, pp. 1483-1494, Jun. 2017.
[15] M. Wang, J. Beerten, and D. van Hertem, "Frequency domain based DC fault analysis for bipolar HVDC grids," *Journal of Modern Power Systems and Clean Energy*, vol. 5, no. 4, pp. 548-559, Jul. 2017.
[16] Z. He, K. Liao, X. Li *et al*., "Natural frequency-based line fault location in HVDC lines," *IEEE Transactions on Power Delivery*, vol. 29, no. 2, pp. 851-859, Apr. 2014.
[17] Y. Liang, G. Wang, and H. Li, "Time-domain fault-location method on HVDC transmission lines under unsynchronized two-end measurement and uncertain line parameters," *IEEE Transactions on Power Delivery*, vol. 30, no. 3, pp. 1031-1038, Jun. 2015.
[18] X. Zhang, N. Tai, Y. Wang *et al*., "EMTR-based fault location for DC line in VSC-MTDC system using high-frequency currents," *IET Generation, Transmission & Distribution*, vol. 11, no. 10, pp. 2499-2507, Jun. 2017.
[19] X. Zhang, N. Tai, X. Zheng *et al*., "Wavelet-based EMTR method for fault location of VSC-HVDC transmission lines," *The Journal of Engineering*, vol. 16, pp. 961-966, Mar. 2019.
[20] J. P. Keshri and H. Tiwari, "Fault location methods in HVDC transmission system – a review," in *Lecture Notes in Electrical Engineering*, vol. 607. Singapore: Springer, 2019, pp. 411-419.
[21] Y. Zhang, Y. Li, J. Song *et al*., "Pearson correlation coefficient of current derivatives based pilot protection scheme for long-distance LCC-HVDC transmission lines," *Electrical Power and Energy Systems*, vol. 116, pp. 1-8, Mar. 2020.
[22] M. Farshad and J. Sadeh, "A novel fault-location method for HVDC transmission lines based on similarity measure of voltage signals," *IEEE Transactions on Power Delivery*, vol. 28, no. 4, pp. 2483-2490, Oct. 2013.
[23] M. Farshad, "Detection and classification of internal faults in bipolar HVDC transmission lines based on *K*-means data description method," *International Journal of Electrical Power and Energy Systems*, vol. 104, pp. 615-625, Jan. 2019.
[24] W. Leterme, S. P. Azad, and D. van Hertem, "A local backup protection algorithm for HVDC grids," *IEEE Transactions on Power Delivery*, vol. 31, no. 4, pp. 1767-1775, Aug. 2016.
[25] S. P. Azad, W. Leterme, D. van Hertem, "Fast breaker failure backup protection for HVDC grids," *Electric Power Systsems Research*, vol. 138, pp. 99-105, Sept. 2016.
[26] J. Izykowski, R. Molag, E. Rosolowski *et al*., "Accurate location of faults on power transmission lines with use of two-end unsynchronized measurements," *IEEE Transactions on Power Delivery*, vol. 21, no. 2, pp. 627-633, Apr. 2006.
[27] J. Suonan, S. Gao, G. Song *et al*., "A novel fault-location method for HVDC transmission lines," *IEEE Transactions on Power Delivery*, vol. 25, no. 2, pp. 1203-1209, Apr. 2010.
[28] A. Hossam-Eldin, A. Lotfy, M. Elgamal *et al*., "Combined traveling wave and fuzzy logic based fault location in multi-terminal HVDC systems," in *Proceedings of the IEEE 16th International Conference on Environment and Electrical Engineering (EEEIC)*, Florence, Italy, Jun. 2016, pp. 1-6.
[29] V. L. Merlin, R. C. D. Santos, S. L. Blond *et al*., "Efficient and robust ANN-based method for an improved protection of VSC-HVDC systems," *IET Renewable Power Generation*, vol. 12, no. 13, pp. 1555-1562, Aug. 2018.
[30] J. M. Johnson and A. Yadav, "Complete protection scheme for fault detection, classification and location estimation in HVDC transmission lines using support vector machines," *IET Science Measurement Technology*, vol. 11, no. 3, pp. 279-287, May 2017.
[31] R. Muzzammel, "Restricted Boltzmann machines based fault estimation in multi terminal HVDC transmission system," in *Communications in Computer and Information Science*, vol. 1198. Singapore: Springer, 2020, pp. 772-790.
[32] R. Salakhutdinov, A. Mnih, and G. Hinton, "Restricted Boltzmann machines for collaborative filtering," in *Proceedings of the 24th International Conference on Machine Learning*, Corvallis, USA, Jun. 2007, pp. 1-8.
[33] G. E. Hinton and R. Salakhutdinov, "Reducing the dimensionality of data with neural networks," *Science*, vol. 313, pp. 504-507, Jul. 2006.
[34] Y. W. Teh and G. E. Hinton, "Rate-coded restricted Boltzmann machines for face recognition," in *Proceedings of Advances in Neural information Processing Systems 13*. Cambridge: MIT Press, 2000, pp. 1-7.
[35] S. Jian, J. Jiang, K. Lu *et al*., "SEU-tolerant restricted Boltzmann machine learning on DSP-based fault detection," in *Proceedings of 2014 12th International Conference on Signal Processing (ICSP)*, Hangzhou, China, Oct. 2014, pp. 1503-1506.
[36] T. Pan, J. Chen, J. Pan *et al*., "A deep learning network via shunt-wound restricted Boltzmann machines using raw data for fault detection," *IEEE Transactions on Instrumentation and Measurement*, vol. 69, no. 7, pp. 4852-4862, Jul. 2020.
[37] P. Peng, Y. Wu, Y. Zhang *et al*., "A novel fault detection and diagnosis method based on Gaussian-Bernoulli restricted Boltzmann machine," in *Proceedings of 2019 IEEE International Conference on Systems, Man and Cybernetics (SMC)*, Bari, Italy, Oct. 2019, pp. 1349-1354.
[38] S. H. Walker and D. B. Duncan, "Estimation of the probability of an event as a function of several independent variables," *Biometrika*, vol. 54, no. 2, pp. 167-178, Jun. 1967.
[39] D. R. Cox, "The regression analysis of binary sequences (with discussion)," *Journal of the Royal Statistical Society Series B*, vol. 20, no. 2, pp. 215-242, Mar. 1958.
[40] R. Raina, A. Battle, H. Lee *et al*., "Self-taught learning: transfer learning from unlabeled data," in *Proceedings of the 24th International Conference on Machine Learning (ICML)*, Corvallis, USA, Jun. 2007, pp. 759-766.
[41] C. M. Bishop, *Pattern Recognition and Machine Learning*. New York: Springer, 2006, pp 205-213.
[42] G. E. Hinton, "Training products of experts by minimizing contrastive divergence," *Neural Computation*, vol. 14, no. 8, pp. 1771-1800, Aug. 2002.
[43] A. Raza, D. Xu, Y. Liu *et al*., "Coordinated operation and control of VSC based multi-terminal high voltage DC transmission systems," *IEEE Transactions on Sustainable Energy*, vol. 7, no. 1, pp. 364-373, Jan. 2016.

Raheel Muzzammel received the B. Sc. degree in electrical engineering from the University of Engineering and Technology, Lahore, Pakistan, in 2010, and the M.Sc. degree in electrical engineering from the University of Lahore, Lahore, Pakistan, in 2013. He is currently working as an Assistant Professor in the University of Lahore. His research interests include HVDC transmission systems, FIC, FL, relay algorithms, and DC grid protection and machine learning.

Ali Raza received the B. Sc. and M. Sc. degrees in electrical engineering from the University of Engineering and Technology, Lahore, Pakistan, in 2010 and 2013, respectively. He received Ph. D. degree in electrical engineering from Harbin Institute of Technology, Harbin, China, in 2016. Currently, he is attached with the Department of Electrical Engineering, University of Lahore, Lahore, Pakistan, as an Assistant Professor. His research interests include operation and control of M-VSC-HVDC including its effects on power systems, protection, optimization and topological evaluation of MT-HVDC transmission systems for large offshore wind power plants.